Evaluating LSM-Based Water Budgets over a West African Basin Assisted with a River Routing Scheme

Augusto Getirana, Aaron Boone, Christophe Peugeot

Evaluating LSM-Based Water Budgets over a West African Basin Assisted with a River Routing Scheme

AUGUSTO C. V. GETIRANA* AND AARON BOONE

CNRM-GAME, Météo-France, Toulouse, France

CHRISTOPHE PEUGEOT

Hydrosciences, Montpellier, France

(Manuscript received 10 January 2014, in final form 9 July 2014)

ABSTRACT

Within the framework of the African Monsoon Multidisciplinary Analysis (AMMA) Land Surface Model Intercomparison Project phase 2 (ALMIP-2), this study evaluates the water balance simulated by the Interactions between Soil, Biosphere, and Atmosphere (ISBA) over the upper Ouémé River basin, in Benin, using a mesoscale river routing scheme (RRS). The RRS is based on the nonlinear Muskingum–Cunge method coupled with two linear reservoirs that simulate the time delay of both surface runoff and base flow that are produced by land surface models. On the basis of the evidence of a deep water-table recharge in that region, a reservoir representing the deep-water infiltration (DWI) is introduced. The hydrological processes of the basin are simulated for the 2005–08 AMMA field campaign period during which rainfall and streamflow data were intensively collected over the study area. Optimal RRS parameter sets were determined for three optimization experiments that were performed using daily streamflow at five gauges within the basin. Results demonstrate that the RRS simulates streamflow at all gauges with relative errors varying from −20% to 3% and Nash–Sutcliffe coefficients varying from 0.62 to 0.90. DWI varies from 24% to 67% of the base flow as a function of the subbasin. The relatively simple reservoir DWI approach is quite robust, and further improvements would likely necessitate more complex solutions (e.g., considering seasonality and soil type in ISBA); thus, such modifications are recommended for future studies. Although the evaluation shows that the simulated streamflows are generally satisfactory, further field investigations are necessary to confirm some of the model assumptions.

1. Introduction

The AMMA (African Monsoon Multidisciplinary Analysis) project (Redelsperger et al. 2006) was implemented with the main goal of acquiring a better understanding of the intraseasonal and interannual variability of the West African monsoon. The study of the terrestrial water budget has been one of the key research topics of the project. While significant progress was made in terms of both basic understanding and modeling, questions still linger concerning the impact of land surface and hydrological processes on the monsoon system through feedback mechanisms and the capacity of current Earth system models to represent physical processes in that area. This is critical since there is a need to better quantify both current and future water availability within the context of predicted climate change over an already water resource–limited region. The AMMA Land Surface Model Intercomparison Project (ALMIP; Boone et al. 2009b) was developed within AMMA in order to evaluate the representation of the water and energy cycles in the current generation of land surface models (LSMs) over West Africa. Other goals of ALMIP are the identification of possible missing processes in LSMs and the forcing of state-of-the-art LSMs with high-quality and relatively high spatiotemporal-resolution data in order to better understand the key processes and their corresponding scales.

ALMIP is subdivided into two phases. ALMIP phase 1 (ALMIP-1; Boone et al. 2009b) focused on the regional

* Current affiliation: NASA Goddard Space Flight Center, Greenbelt, Maryland.

Corresponding author address: Augusto Getirana, NASA Goddard Space Flight Center, 8800 Greenbelt Rd., Greenbelt, MD 20771.
E-mail: augusto.getirana@nasa.gov

DOI: 10.1175/JHM-D-14-0012.1

scale with a domain that covers most of West Africa at a 0.5° spatial resolution, and ALMIP phase 2 (ALMIP-2; Boone et al. 2009a) deals with the local and mesoscales. Twenty land surface and hydrological models are intercompared and evaluated over this region using observational data from three heavily instrumented supersites from the AMMA–Coupling the Tropical Atmosphere and the Hydrological Cycle (AMMA-CATCH; Lebel et al. 2009) observing system. These supersites, located in Mali, Niger, and Benin, are located along a north–south transect and therefore provide a good characterization of the West African ecoclimatic gradient. The current study focuses on the upper Ouémé River basin, located in Benin, in which river networks are well structured. Over the other two mesoscale supersites, both gullies of limited extension (1–10 km) and low connectivity transfer water to topographic depressions (sinks), with no flow at larger scales (so-called endorheism; Desconnets et al. 1997). The mesoscale modeling of the water cycle in such a complex context is beyond the scope of this study, even though it will be considered in future works. Previous modeling studies over this region have used conceptual and physically based hydrological models in order to reproduce streamflow at gauges (e.g., Varado et al. 2006; Giertz et al. 2006; Le Lay et al. 2008; Gaiser et al. 2008). Compared to typical hydrological models, LSMs generally have detailed representations of near-surface hydrology, soil properties, and vegetation processes, while neglecting or parameterizing lateral flow processes. A straightforward way to evaluate the water budget provided by hydrological models is to compare observed and simulated river streamflow (e.g., Lohmann et al. 1998; Getirana et al. 2014), as it can be directly measured, with cost-effective methods, in almost any basin. Streamflow results from the combination of various processes within the basin (surface, subsurface transfer, groundwater discharge, and routing in open channel networks); thus, it provides useful information for evaluating the overall water cycle in spatially distributed models.

Recent advances from field campaigns and modeling over the ALMIP area have provided evidence that most of the streamflow originates from perched water tables. It develops in the near surface (1–2 m), with almost no contribution from the underlying (10–15 m deep) permanent water table (Kamagaté et al. 2007; Séguis et al. 2011). This permanent water table is seasonally recharged by deep infiltration in the rainy season. In the absence of evidence for large-scale flow in the permanent water table, or a significant contribution to the rivers, dry-season evapotranspiration (ET) is assumed the main cause of groundwater depletion (Descloitres et al. 2011; Richard et al. 2013). In this context, the ALMIP-2 River Routing Scheme (ARTS) was developed in order to simulate the partitioning and transfer of surface and base flow simulated by LSMs. ARTS is composed of two modules: 1) two linear reservoirs representing the time delay to reach the river network for both surface runoff and base flow in each grid cell (i.e., the time delay corresponds to the time needed for the water to flow from the headwater grid cell to the river) and 2) a flow routing routine based on the nonlinear Muskingum–Cunge (MC) method (Ponce 1989). The first module is used to partition base flow between water-table recharge and lateral fluxes to the river. ARTS is therefore more than strictly a river routing scheme; it can be viewed as a hydrologic postprocessor that accounts for both surface water and groundwater dynamics. In this study, the near-surface water budget is simulated by the Interactions between Soil, Biosphere, and Atmosphere (ISBA) model (Noilhan and Mahfouf 1996). Surface runoff and base flow simulated by ISBA are used as forcing in ARTS to generate streamflow and groundwater recharge. Most ARTS parameters can be acquired from in situ observations and/or satellite imagery. However, the determination of four model parameters requires either expertise or automatic calibration. Three of them are related to time delays or deep-water infiltration (DWI) rates, while the fourth parameter is the so-called Manning's roughness coefficient that is required for the MC-based scheme.

In addition to describing the ARTS scheme, the main objectives of this study are 1) to evaluate the ability of ISBA to simulate the mesoscale hydrology in that region, given its relatively simple and standard representation of such processes, and 2) to investigate possible structural biases in LSMs that result from the inadequate or missing representation of some key processes. The latter objective is attained through the use of ARTS parameters. In this sense, parameters are estimated through three automatic calibration experiments, each considering a set of streamflow datasets that differ from each other according to the number and order of gauges that are used in the optimization process. The University of Arizona multiobjective complex evolution (MOCOM-UA) global optimization algorithm (Yapo et al. 1998) is considered in this context.

This study is a test bed for a forthcoming multi-LSM evaluation based on the ALMIP-2 ensemble simulations. This paper is organized into four sections. Section 2 presents the study area and a description of the available datasets. Section 3 provides the modeling approach, including a detailed description of ARTS and the MOCOM-UA algorithm, as well as the experimental design. In section 4, the results are shown, compared, and discussed, and section 5 presents the concluding remarks.

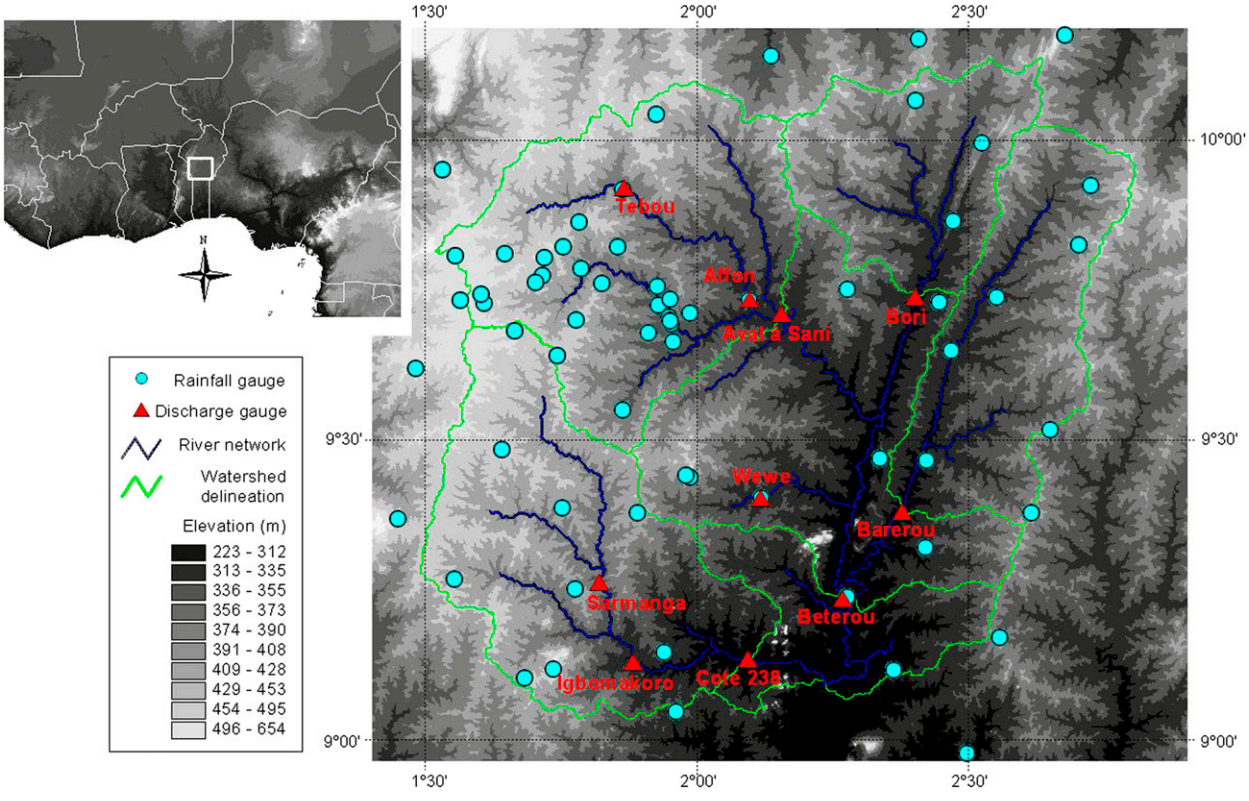

FIG. 1. Location of the upper Ouémé River basin.

2. Study area

The upper Ouémé River basin is located in northern Benin, with a drainage area of ~14 400 km^2 (see Fig. 1). It is one of the three ALMIP-2 meso sites (also including the Mali and Niger meso sites; Boone et al. 2009a) and the only one with available streamflow observations at that scale. The basin is located within the Sudanian climatic regime, and it is characterized by a single rainy season with an average rainfall of ~1150 mm yr^{-1}. The bulk of the rainfall occurs during the monsoon, which corresponds to the period between April and October (approximately 60% of the rain falls between July and September). More details about the rainfall characteristics in the region can be found in Depraetere et al. (2009). The streamflow is intermittent, occurring between the end of June and January. The basinwide average runoff (estimated from observations between 2005 and 2008, for which data are available for this study) is approximately 150 mm yr^{-1}, and this corresponds to a runoff ratio (runoff/rainfall) of approximately 0.12. These ratios can vary spatially from 0.08, at Bori station, to 0.24, at Tebou station (see locations in Fig. 1). According to previous studies based on observed data (Kamagaté et al. 2007; Séguis et al. 2011), recharge rates range from 10% to 17% of the annual rainfall depending on the year.

a. *Meteorological forcing*

A dense rainfall gauge network maintained by the AMMA-CATCH observing system (Lebel et al. 2009) is available over the study area (see Fig. 1 for the rainfall gauge distribution). The rainfall product used in this study is derived from an interpolation technique based on a combined krigged–Lagrangian methodology (Vischel et al. 2009). The resulting rainfall product is available at a 30-min time step for the 2005–08 period at a 0.05° spatial resolution. Surface parameters, such as the leaf area index (LAI) and albedo, are from the ECOCLIMAP2 database (Kaptué Tchuenté et al. 2011). Note that, unlike ALMIP-1, ALMIP-2 input vegetation parameters include interannual vegetation variability. This dataset was developed specifically for applications such as ALMIP-2 since the vegetation is characterized at very large interannual variability over this region. Mesoscale downwelling fluxes (interpolated from a 3-km resolution grid to a 0.05° spatial resolution and aggregated from a 15- to a 30-min time step for this project) are from the Land Surface Analysis Satellite Applications Facility (LandSAF) project (Geiger et al. 2008; Trigo et al. 2011). Other meteorological forcings are derived from the European Centre for Medium-Range Weather Forecasts (ECMWF) operational forecast system [for

TABLE 1. Selected streamflow gauges located within the upper Ouémé River basin.

Station name	Lat (°)	Lon (°)	Area (km^2)	Observed discharge ($m^3 s^{-1}$)	Observed runoff rate ($mm\ day^{-1}$)	Rainfall ($mm\ day^{-1}$)	Runoff ratio (runoff/rainfall)
Beterou	9.20	2.27	10 140	43.13	0.37	3.01	0.12
Aval-Sani	9.72	2.15	3307	17.54	0.46	2.99	0.15
Bori	9.76	2.40	1630	4.86	0.26	2.98	0.09
Barerou	9.36	2.38	2141	8.03	0.32	3.07	0.10
Cote 238	9.09	2.09	3152	17.61	0.48	3.13	0.15
Igbomakoro	9.08	1.88	2335	13.96	0.52	3.01	0.17
Sarmanga	9.23	1.82	1371	9.90	0.62	3.06	0.20
Affon	9.75	2.10	1187	6.56	0.48	3.08	0.15
Tebou	9.96	1.86	533	4.57	0.74	3.10	0.24

further details, see Boone et al. (2009a)], with relatively small hypsometric-based adjustments to the temperature, specific humidity, and surface pressure using the differences between the large-scale model and ALMIP-2 mesoscale topography.

b. *Streamflow*

The streamflow observations at 10 gauges (see locations in Fig. 1) maintained by the AMMA-CATCH observing system were utilized in the modeling experiments described below. The five main catchments within the basin (Beterou, Aval-Sani, Bori, Barerou, and Cote 238) were used in the parameter calibration (described in the next section) and the other four (Igbomakoro, Sarmanga, Affon, and Tebou) were used for the parameter evaluation. The drainage areas vary from 533 km^2 (Tebou station) to 10 140 km^2 (Beterou station), with mean streamflow ranging from 1.3 to 43.1 $m^3 s^{-1}$. The main characteristics of the catchments (identified by the corresponding gauges) are listed in Table 1.

The river length and slope, flow direction, and drainage area used in river routing scheme were derived from Shuttle Radar Topography Mission (SRTM; Farr et al. 2007) digital elevation model (DEM) data processing. Cross-sectional observations at 12 gauges were used to determine river widths as a function of the drainage area based on a power-law relation. The power-law method used herein is widely cited in the literature (e.g., Coe et al. 2008; Getirana et al. 2010; Decharme et al. 2012; Li et al. 2013), and it has been shown to be able to provide reasonable spatially distributed estimates of river geometry in different areas in the world.

3. Modeling approach

This section provides a detailed description of the ARTS parameterization and the land surface hydrology module in ISBA. The MOCOM-UA (Yapo et al. 1998) optimization algorithm used for the ARTS calibration is briefly presented [detailed descriptions are presented in Yapo et al. (1998) and Boyle et al. (2000)]. ISBA and ARTS were coupled in offline mode, that is, ARTS was run using ISBA outputs (surface runoff and base flow) as input data.

a. *The ARTS river routing scheme*

ARTS is a mesoscale river routing scheme developed in the framework of the ALMIP-2 project with the objective of evaluating the water budget provided by multiple LSMs. Surface runoff R and baseflow B components generated by an LSM at each grid cell are routed through the river network using the nonlinear MC method. This method provides a numerical solution similar to the diffusion term of the Saint Venant equation. The model simulates daily spatially distributed streamflow with internal computational time steps that can be adjusted for accuracy (varying from a few minutes to several hours) as a function of the river reach length, river bed slope, and kinematic wave celerity. The spatial resolution of both ARTS and ISBA in the current study is 0.05° × 0.05°, which results in 473 grid cells for the upper Ouémé River basin.

ARTS also represents the R and B time delays before reaching the river network using a linear reservoir approach. The methodology is similar to that used in the Hydrological Modeling and Analysis Platform (HyMAP; Getirana et al. 2012), except for the fact that ARTS is capable of simulating the deep-water infiltration, as described in the next sections. The surface runoff time delay τ_r is the product of a spatially distributed surface runoff time delay factor, determined by the Kripich (1940) formula, and a spatially uniform parameter. The baseflow time delay τ_b is calibrated. In addition, ARTS can represent water losses and water-table recharge via deep-water infiltration. At each time step, a uniform and constant fraction of the base flow is diverted to the aquifer reservoir. The remaining fraction, transferred to the river, mimics the subsurface flow that is not specifically diagnosed by most LSMs. A schematic of the model is shown in Fig. 2.

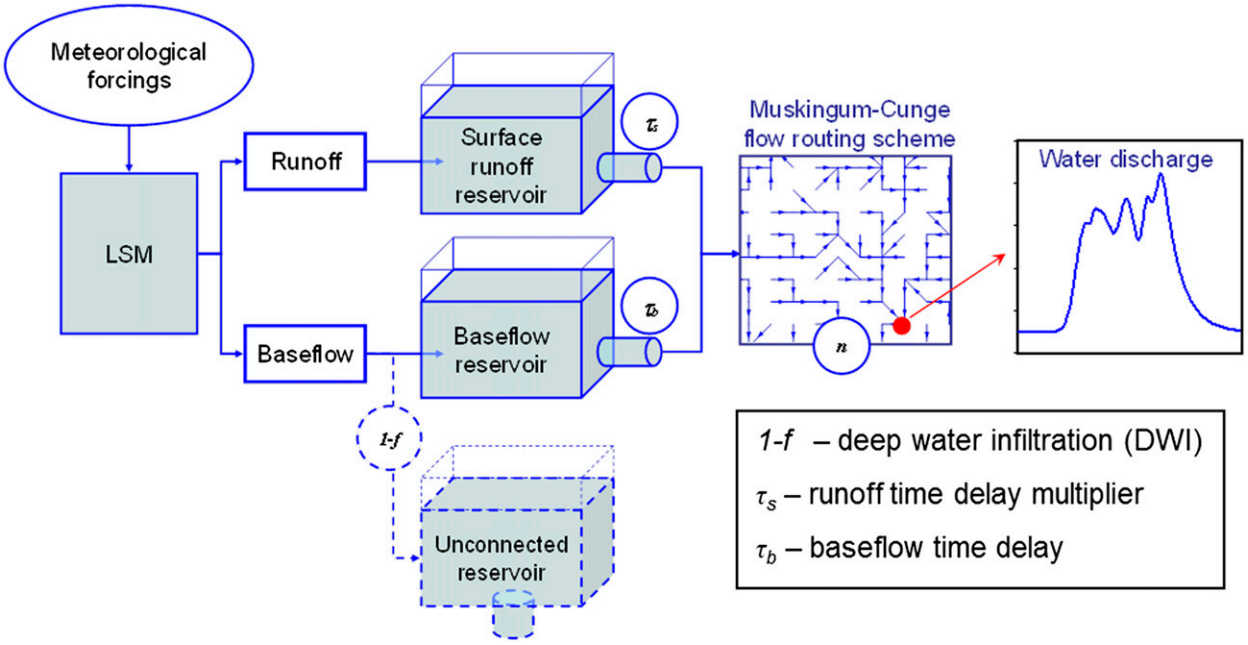

FIG. 2. Schematic of the ARTS river routing scheme.

1) THE RUNOFF AND BASEFLOW TIME DELAYS

As mentioned above, R (mm Δt^{-1}) and B (mm Δt^{-1}) derived from an LSM are used as inputs for an ARTS simulation. At each time step, a fraction f of B, called subsurface flow B' ($B' = Bf$), is transferred to the river network while the remaining part, referred to as deep-water infiltration [DWI = $B(1 - f)$], leaves the system to an assumed deep aquifer. The fraction f is calibrated in order to fit mean observed and simulated streamflow. Note that feedbacks from this deep aquifer to both soils and rivers seem to be negligible, even over time scales longer than the one considered in this study (Leduc et al. 1997; Séguis et al. 2011), thereby enforcing the fraction f assumption for this study.

The time delay characterizes a physically based process that represents the subgrid-scale routing (Getirana et al. 2012). For each grid cell, R and B' (mm Δt^{-1}) pass through separate linear reservoirs. The time delay of each linear reservoir can vary from a few hours to several days, depending on the hydrogeological characteristics of the catchment. The linear reservoir outflows can be represented by

$$O_{r,b} = \frac{V_{r,b}}{\tau_{r,b}}, \tag{1}$$

where the subscripts r and b represent surface runoff and baseflow variables, respectively. The variable $O_{r,b}$ (mm Δt^{-1}) stands for the outflow at time step t, $V_{r,b}$ (mm) represents the water stored in the linear reservoir, and $\tau_{r,b}$ (Δt) is the depletion rate of linear reservoirs that is determined as a function of the time delay factor of a grid cell. The variable V is updated twice at each time step: at the beginning, adding the inflows R and B' and at the end, by subtracting $O_{r,b}$. The τ_b parameter can be defined as a function of hydrogeological characteristics of the basin, and it represents the depletion rate of the baseflow linear reservoirs. Some studies suggest that it can be derived from the recession time of observed hydrographs at the catchment outlet (e.g., Collischonn et al. 2007). In ARTS, τ_b is assumed to be spatially uniform and constant in time, and it is calibrated. The surface runoff transfer time scale τ_r is spatially distributed and defined as

$$\tau_{r_j} = T_{r_j} p_r, \tag{2}$$

where T_r (Δt) is a surface runoff time delay factor for each grid cell and p_r is a spatially uniform parameter. The variable T_r is computed for each grid cell j from Kirpich (1940):

$$T_{r_j} = 3600 \left(0.868 \frac{\Delta x_j^3}{\Delta h_j} \right)^{0.385}, \tag{3}$$

where Δx_j (km) is the distance between the farthest point within a grid cell and its outlet and Δh_j (m) is the difference between the maximum and minimum elevations of the pathway. Both Δx_j and Δh_j are derived from a high-resolution DEM. Finally, the total streamflow Q_c (m^3 Δt^{-1}) produced in each grid cell is computed as

$$Q_c = (O_r + O_b)A_c, \quad (4)$$

where A_c (m^2) stands for the grid cell area.

2) WATER FLOW IN THE RIVER NETWORK

The Muskingum–Cunge routing method is based on the equation

$$\mathrm{Qo}^{t+1} = C_1\mathrm{Qi}^t + C_2\mathrm{Qi}^{t+1} + C_3\mathrm{Qo}^t, \quad (5)$$

where, for each grid cell, Qo^{t+1} ($m^3\,\Delta t^{-1}$) is the outflow at time step $t + 1$, Qo^t ($m^3\,\Delta t^{-1}$) is the outflow at time step t, Qi^t ($m^3\,\Delta t^{-1}$) is the inflow at time step t, and Qi^{t+1} ($m^3\,\Delta t^{-1}$) is the inflow at time step $t + 1$. The variables Qo^t and Qi^t result from the preceding time step computation, and Qi^{t+1} is the summation of the streamflow produced in the current grid cell and the outflow of upstream grid cells i:

$$\mathrm{Qi}^{t+1} = \mathrm{Qc}^{t+1} + \sum_{i=1}^{\mathrm{nUp}} \mathrm{Qc}_i^{t+1}, \quad (6)$$

where nUp represents the number of upstream grid cells.

The variables C_1, C_2, and C_3 are defined as

$$C_1 = \frac{2KX + \Delta t'}{2K(1-X) + \Delta t'}, \quad (7)$$

$$C_2 = \frac{\Delta t' - 2KX}{2K(1-X) + \Delta t'}, \quad (8)$$

and

$$C_3 = \frac{2K(1-X) - \Delta t'}{2K(1-X) + \Delta t'}, \quad (9)$$

where $\Delta t'$ is a submultiple of the model time step. The variables K and X are physically based constants, also known as the variable parameters of the MC method (Ponce 1989):

$$K = \frac{\Delta x'}{c_o} \quad (10)$$

and

$$X = \frac{1}{2} - \frac{q_o}{wS_o c_o \Delta x'}, \quad (11)$$

where c_o ($m\,s^{-1}$) stands for the kinematic wave celerity, q_o ($m^3\,s^{-1}$) is the water discharge of reference, and S_o and w (m) are the river bed slope and width of the main river reach within the grid cell. The variable $\Delta x'$ (m) is the length of a river reach, which can be a submultiple of the total river length within the grid cell. The variable c_o is computed as

$$c_o = \frac{5}{3}\frac{q_o^{0.4}S_o^{0.3}}{n^{0.6}w^{0.4}}, \quad (12)$$

where n is the Manning roughness coefficient and estimates are available in the literature for most flow regimes and different river physical characteristics (Chow 1988). In this study, n has been defined as being spatially uniform and constant in time (equal to 0.03), which is in agreement with values suggested in the literature (Chow 1988) for the physical characteristics of rivers found in this basin.

The variable S_o is approximated as the valley slope, which is derived from the SRTM DEM. The variable w (m) was derived from a power-law equation as a function of the drainage area A (km^2), based on the observed river widths at the corresponding gauges. The following equation was used to derive a map of w within the basin:

$$w = 12.A^{0.17} \quad R^2 = 0.69. \quad (13)$$

The nonlinear version of the MC method is used in this study, which means that the kinematic wave celerity varies with discharge. This version of the MC method is particularly useful for long reaches and rivers with a wide range of flow-level variation (Ponce 1989). The nonlinearity of the MC method is introduced by varying the routing parameters X and K. These parameters are functions of q_o and c_o, which are computed with a three-point average of the known values. Thus, q_o for the time step $t + 1$ is provided by

$$q_o^{t+1} = \frac{\mathrm{Qi}^t + \mathrm{Qi}^{t+1} + \mathrm{Qo}^t}{3}. \quad (14)$$

Ponce and Yevjevich (1978) showed that this equation provides satisfactory estimates of q_o when compared to the interactive four-point average method, which includes the unknown variable Qo^{t+1}.

The MC method provides an optimal precision when the following relation is satisfied (Tucci 1998):

$$\frac{q_o}{wS_o c_o} + 0.8(c_o\Delta t')^{0.8}(\Delta x')^{0.2} - \Delta x' = 0. \quad (15)$$

Optimal submultiples of the river length in a computational cell $\Delta x'$ and model time step interval $\Delta t'$ are calculated using the Newton–Raphson method applied to Eq. (15). This improves the precision of the wave propagation within the grid cells. To solve Eq. (5), the parameters K and X [Eqs. (10) and (11)] are calculated based on geomorphologic characteristics of the study area. The physical basis of these parameters distinguishes the MC method from the Muskingum method, which

estimates K and X empirically. Most of these data can be easily derived from satellite or in situ observations.

b. The ISBA land surface model

ISBA is a state-of-the-art LSM that is a part of the Surface Externalized (SURFEX) platform (Masson et al. 2013). The model is used for operational numerical weather prediction, global climate model simulations, operational hydrological forecasting over France, offline land data assimilation applications, and mesoscale atmospheric research modeling [see Masson et al. (2013) for a review of the different applications]. ISBA provides fluxes of mass, heat, carbon, radiation, and momentum to the overlying atmosphere (in coupled mode), in addition to predicting the temporal evolution of the near-surface continental water and energy balance components and surface state variables (in coupled or offline mode). ISBA contains many physics options for soil, snow cover, and photosynthesis, the choice of which depends on a given application.

LAND SURFACE MODEL HYDROLOGY

Within ISBA, there are several different hydrological parameterizations available. For example, within the global climate model (large-scale applications), the ISBA–Total Runoff Integrating Pathways (ISBA-TRIP) river routing methodology (Decharme et al. 2012) is used. In the current study at the mesoscale, we use a new approach based on the MC methodology. Compared to the ISBA-TRIP parameterization, this method includes processes that are more amenable to mesoscale hydrodynamics. In terms of near-surface hydrology, a relatively simple and standard three-layer force–restore hydrological configuration is used (Boone et al. 1999). In terms of surface runoff, the variable infiltration capacity methodology is activated (Habets et al. 1999). The hydrological simulations from this configuration have been evaluated at the regional scale within the context of international intercomparison projects (e.g., Boone et al. 2004). The surface runoff is parameterized as

$$Q_{\mathrm{rcrit}} = \left[1 - \frac{(w_2 - w_{\mathrm{rgmin}})}{(w_{\mathrm{sat}} - w_{\mathrm{rgmin}})}\right]^{1/(1+B)} - \frac{R_t \Delta t}{\rho_w d_2}\left[\frac{1}{(1+B)(w_{\mathrm{sat}} - w_{\mathrm{rgmin}})}\right], \quad (16)$$

$$Q_r = R_t - \frac{\rho_w d_2}{\Delta t}\{(w_{\mathrm{sat}} - w_2) - (w_{\mathrm{sat}} - w_{\mathrm{rgmin}})[\max(0, Q_{\mathrm{rcrit}})]^{1+B}\}, \quad (17)$$

and

$$Q_r = 0 \quad \text{if} \quad (Q_r < 0) \quad \text{or} \quad (w_2 - w_{\mathrm{rgmin}} < 0), \quad (18)$$

where Q_{rcrit} ($\mathrm{m^3\,m^{-3}}$) is a critical nondimensional flow rate, w_2 is the volumetric water content of the surface layer, w_{sat} ($\mathrm{m^3\,m^{-3}}$) is the porosity, R_t ($\mathrm{kg\,m^{-2}\,s^{-1}}$) is the throughfall or potential infiltration rate, Δt (s) is the time step, d_2 (m) is the depth of the second (root zone) soil layer, and ρ_w ($1000\,\mathrm{kg\,m^{-3}}$) represents the density of liquid water. The variable B is the so-called variable infiltration parameter, and the current default value of $B = 0.5$ (Habets et al. 1999) is used in this study. The parameter w_{rgmin} ($\mathrm{m^3\,m^{-3}}$) is a threshold volumetric water content that is sufficiently humid to generate surface runoff. By default, w_{rgmin} has been set somewhat arbitrarily (for lack of observational studies) to the wilting point value for large-scale or global modeling applications. But note that the wilting point represents the minimum soil moisture at which plant roots can uptake soil water: strictly speaking, it does not actually have a hydrological significance. In the current study, based on the runoff generation in the beginning of the rainy season, it was found that surface runoff did not occur until the soil was moistened to values above the wilting point (based on streamflow observations). Running ISBA with its default w_{rgmin} results in early runoff generation, which is not consistent with observed streamflow. After some testing, we assigned a constant value that is computed as the average of the wilting point and field capacity to this parameter. This value was found to be quite stable (it produced similar improved results for the 4 years in this study).

c. The MOCOM-UA algorithm

The MOCOM-UA is a global multiobjective optimization algorithm that provides a distribution of solutions on the Pareto optimum space. The algorithm only requires the definition of the population ns of points randomly distributed within the parameter hyperspace. The parameter hyperspace is defined by the n-dimensional feasible parameter space. The population of ns points is ranked and sorted according to a Pareto ranking procedure for each iteration, as suggested by Goldberg (1989). The optimization process stops when the entire population has converged toward the Pareto optimum, that is, when all ns points are ranked evenly. Further details about the MOCOM-UA algorithm can be found in the literature (e.g., Yapo et al. 1997, 1998; Boyle et al. 2000).

d. Experimental design

ARTS was automatically calibrated for the period from 2005 to 2008 using the MOCOM-UA algorithm. Three calibration experiments have been performed,

TABLE 2. Optimal parameter sets obtained in the calibration experiments.

					Experiment 3				
Parameters	First guess	Search domain	Experiment 1	Experiment 2	Aval-Sani	Bori	Barerou	Beterou	Cote 238
τ_b (days)	12.5	0–100	8.0	10.7	1.9	25.9	19.1	8.4	9.4
p_r	50	0–250	32	39	21	100	57	36	33
f (%)	40	0–100	59	57	70	33	61	70	76

differing from each other according to the number of utilized gauges providing streamflow observations and how they were used to drive the optimization algorithm. Experiment 1 only incorporated the Beterou station, with a drainage area of 10 140 km^2, which includes the other three gauges (Aval-Sani, Bori, and Barerou). In experiment 2, data available at the five gauges listed in Table 1 were used in the optimization process simultaneously. At each iteration of experiment 2, objective functions (OFs) are computed as the weighted sum of the performance coefficients at the gauges, represented as (Getirana et al. 2013):

$$\mathrm{OF} = \text{minimize}\left[1 - \frac{\sum_{k=1}^{n} F(O,S,t)W_k}{\sum_{k=1}^{n} W_k}\right], \qquad (19)$$

where F is a performance coefficient that is a function of the time step t and the simulated S and observed O signals, W is the weight attributed to each gauge, and k represents the total number of stations considered in the experiment. The function F can be represented by different performance coefficients.

Finally, in experiment 3, the same five stations were considered, but parameter sets were calibrated for each catchment individually. The upstream catchments were calibrated first, and then selected optimal parameters were used to calibrate parameter sets for the downstream catchments. For all experiments, the Nash–Sutcliffe (NS) coefficient and the normalized root-mean-square error (NRMSE) for streamflow were defined as F:

$$\mathrm{NS} = 1 - \frac{\sum_{t=1}^{\mathrm{nt}} (y_t - x_t)^2}{\sum_{t=1}^{\mathrm{nt}} (y_t - \overline{y})^2} \qquad (20)$$

and

$$\mathrm{NRMSE} = \frac{\mathrm{RMSE}}{(y_{\max} - y_{\min})}, \qquad (21)$$

where t is the time step and nt represents the total number of days with observed data. The variables x and y are, respectively, the simulated and target (observed) signals at time step t, while $y_{\max}$, $y_{\min}$, and $\overline{y}$ represent the maximum, minimum, and mean values of the target signals for the entire period. The term NS ranges from $-\infty$ to 1, where 1 is the optimal case, while 0 results when simulations represent observed signals as well as the mean value. NRMSE varies from -1 to $+\infty$, where 0 is the optimal case.

A manual calibration was performed in order to refine the parameter values. The parameters τ_b, p_r, and f were considered in the optimization procedure, and relatively large parameter domains were defined with the purpose of covering the entire range of feasible values. Table 2 shows the first guess for the automatic calibration. The value of NS was fixed as 200 in the experiments performed in this study. Since the objective of this paper is the presentation and evaluation of ARTS rather than the MOCOM-UA algorithm, details about the optimization efficiency are not presented.

Results were evaluated using two additional coefficients: the relative volume error of the streamflow (RE) and the NS coefficient for seasonal variability (NS_d), as suggested by Schaefli and Gupta (2007):

$$\mathrm{RE} = \frac{\sum_{t=1}^{\mathrm{nt}} x_t - \sum_{t=1}^{\mathrm{nt}} y_t}{\sum_{t=1}^{\mathrm{nt}} y_t} \qquad (22)$$

and

$$\mathrm{NS}_d = 1 - \frac{\sum_{t=1}^{\mathrm{nt}} (y_t - x_t)^2}{\sum_{t=1}^{\mathrm{nt}} (y_t - y_{\mathrm{tref}})^2}, \qquad (23)$$

where y_{tref} is the reference value at time step t. The term RE allows us to determine whether mean simulations under- or overestimate observation while NS_d identifies whenever the model has more predictive abilities than those processes already contained within the seasonality of the reference signal.

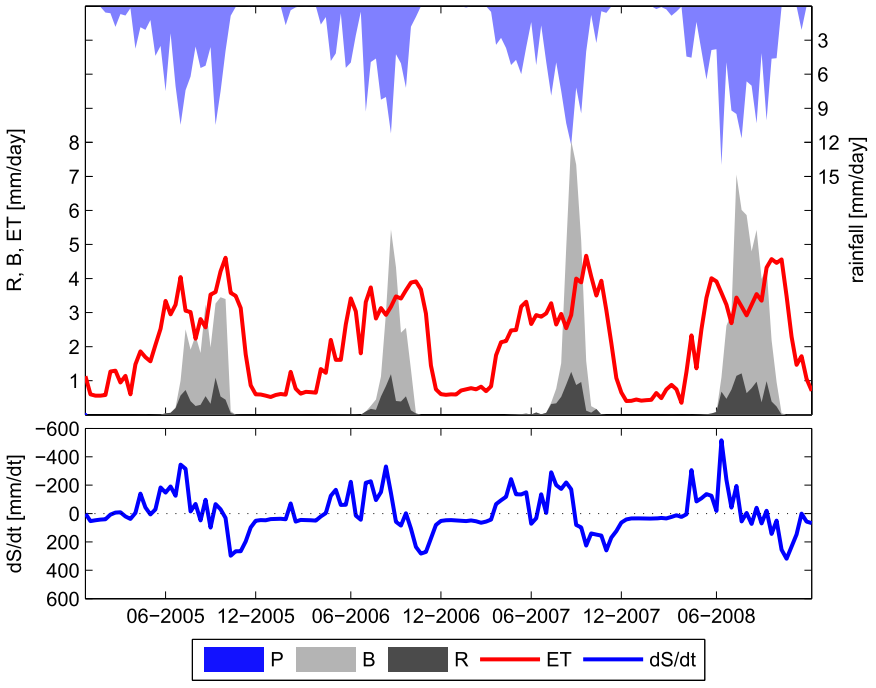

FIG. 3. The 10-day time step series of precipitation (P); simulated ET, R, and B; and change of the water storage in the soil (dS/dt) averaged over the entire basin.

4. Results and discussion

a. Water budget simulated by ISBA

The basinwide average ET simulated by ISBA can reach daily values as high as 7 mm day^{-1} during the rainy season, with a considerable decrease during the dry season: values as low as 0.4 mm day^{-1} are produced during this period (the time series for the water budget components are shown in Fig. 3). Runoff starts to occur about 3 months after the rainy season starts. Approximately 72% (2.15 mm day^{-1}) of the precipitation within the basin is lost through ET, while 5% and 23% are converted into surface runoff (0.17 mm day^{-1}) and base flow (0.68 mm day^{-1}), respectively. The total runoff simulated by ISBA is found to significantly overestimate the observed streamflow. This is consistent with the findings of previous studies suggesting the occurrence of a deep-water infiltration in the studied area (Séguis et al. 2011). The overestimation varies from ~190% at the Aval-Sani station to ~330% at the Bori station. In contrast, if only the surface runoff is considered, there is an underestimation that varies from 37% at Bori station to 64% at Aval-Sani, as shown in Fig. 4. These significant differences suggest a limited representation of hydrological processes in ISBA. The water balance is first evaluated in terms of ET, which is justified by the hypothesis that underestimating the simulated total ET can result in increased total runoff rates. This hypothesis

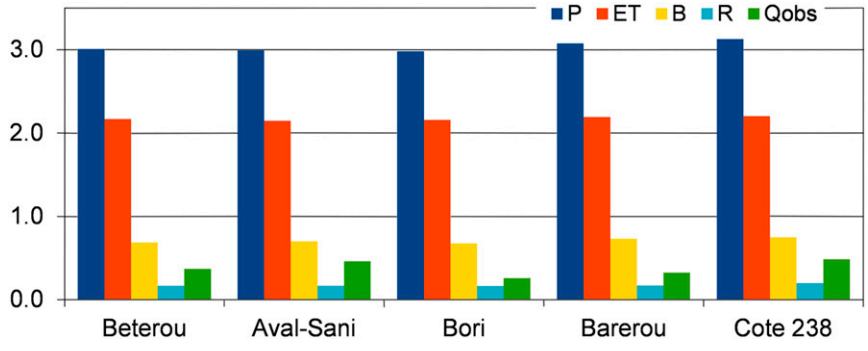

FIG. 4. Water balance variables (P, ET, B, R, and observed streamflow Q_{obs}) averaged over the 2005–08 period (mm day^{-1}).

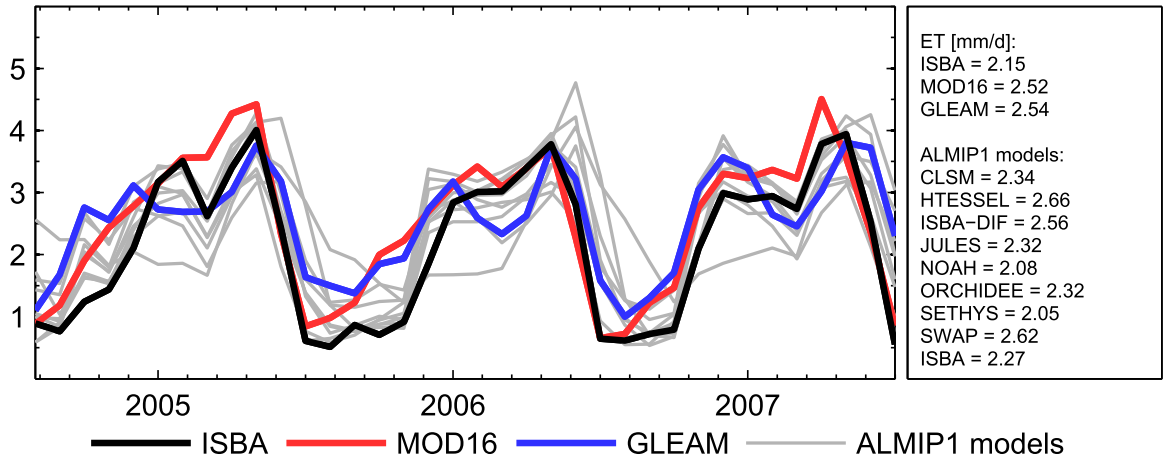

FIG. 5. Monthly ET in the upper Ouémé River basin from 2005 to 2007 derived from ISBA parameterized as described in this study, MOD16 (Mu et al. 2007, 2011), GLEAM (Miralles et al. 2011), and ALMIP-1 LSM outputs. Values on the right correspond to the averages of time series.

is sustained by the possible existence of deep tree roots in the studied area. According to Canadell et al. (1996), tree roots can reach 4–15-m depths in tropical areas. On the other hand, input ECOCLIMAP soil parameters specify approximately 1–2-m soil depths in the basin (and the corresponding prescribed rooting depths are even less), while in situ observations in this basin (unpublished data) suggest that tree roots extend much deeper than the rooting depth prescribed in current LSMs. As a result, it is expected that models underestimate ET during the dry season. Evidently, other hypotheses, such as the misrepresentation of the deep aquifer infiltration, are also potential explanations for the total runoff overestimation.

Simulated ET was evaluated by comparing it against ALMIP-1 LSM outputs (Boone et al. 2009b) and two other satellite-based products: the Moderate Resolution Imaging Spectroradiometer (MODIS)-based ET dataset (MOD16; Mu et al. 2007, 2011) and the Global Land-Surface Evaporation: the Amsterdam Methodology (GLEAM; Miralles et al. 2011). Trambauer et al. (2014) performed a comparison of numerous ET products, including MOD16 and GLEAM, demonstrating that they agree well with other datasets describing the study area. Figure 5 shows the monthly time series of these products from 2005 to 2007. According to the figure, all ET estimates exhibit similar seasonality, but a wide range of values in both dry and wet seasons is perceptible. However, it should be noted that ISBA tends to underestimate ET, if compared to the satellite-based estimates, by about 15%, which is mostly caused by an early rise in the beginning of the rainy season. This could be explained by the aforementioned shallow root zone (1–2 m) found in most LSMs, including ISBA. This results in low groundwater availability, especially during the dry season. But this difference corresponds to only about half of the difference between total runoff and observed discharge. Excessive total runoff can also be due to the overestimation of the rainfall used for model forcing. However, this is deemed to be unlikely to explain the large runoff biases owing to the spatial density of the rain gauges, and the fact that the rain field products have been extensively validated (Vischel et al. 2009). These analyses suggest that neither simulated ET nor rainfall can fully explain the difference between the total runoff and the observed discharge. Assuming that the simulated R correctly represents the actual process, Fig. 4 suggest that only a fraction of the base flow should contribute to the river, which is consistent with field results. Accordingly, the remaining fraction should be abstracted from the surface water cycle and supply a new reservoir, acting as a sink term in the system. These results justify the structure of the ARTS scheme, which allow us to "fix" the LSM simulation by adding these missing processes.

b. *Evaluation of simulated streamflow*

On average, a single run for 473 grid cells and 4 years at the daily time step takes about 1–2 s using an Intel Core 2 Duo 2.4-GHz 4-GB processor under a Linux operating system. In addition, simulations show that ISBA-ARTS can satisfactorily simulate the streamflow in the upper Ouémé River basin, in particular, the 3-month delay between the beginning of the rainy season and the streamflow peaks. Although ISBA outputs overestimate the total runoff within the basin, the inclusion of a reservoir representing the deep-water infiltration significantly reduced these differences, thereby producing simulated streamflow fairly close to the observations using a limited set of calibrated parameters. Figures 6–8 present daily

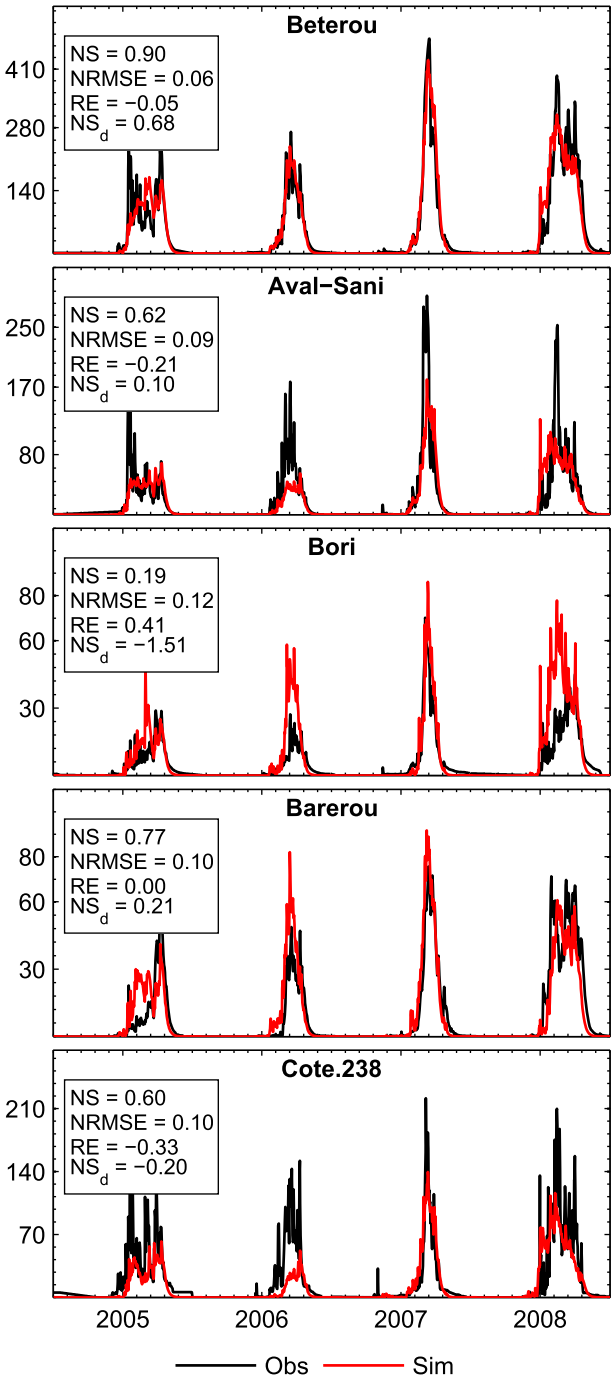

FIG. 6. (from top to bottom) Results at five gauging stations for experiment 1 (calibration with streamflow data observed at the Beterou station).

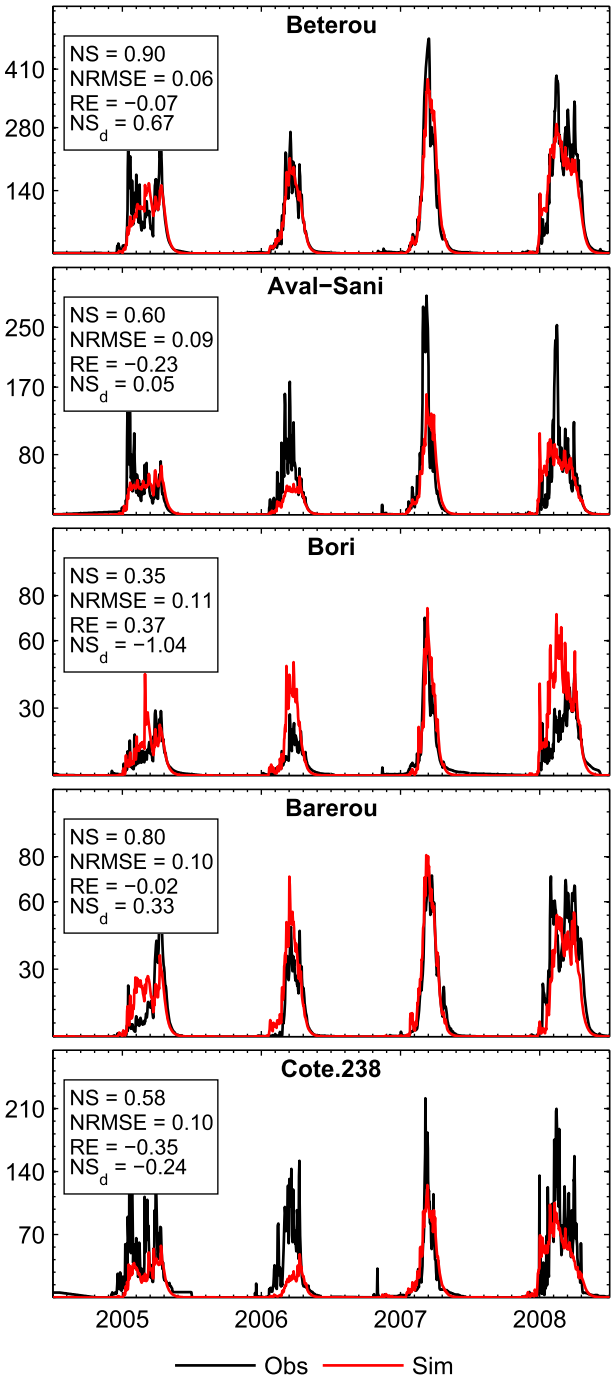

FIG. 7. As in Fig. 6, but for experiment 2 (i.e., calibration with observed streamflow data at five gauging stations simultaneously).

streamflow and performance coefficients of optimal results at the five gauges used in the three optimization experiments. Beterou station, draining most of the basin ($\sim$10 140 km^2), had NS = 0.90 and NRMSE = 0.06 for all of the experiments, with quantitatively comparable RE and NS$_d$ values. Experiments 2 and 3 resulted in −1% and 0.67 for the last two coefficients, respectively, while experiment 1 produced values of −5% and 0.68. Although the coefficients at Beterou are very similar in the three optimization experiments, other stations had varying performances as a function of the number of stations used in the automatic calibration.

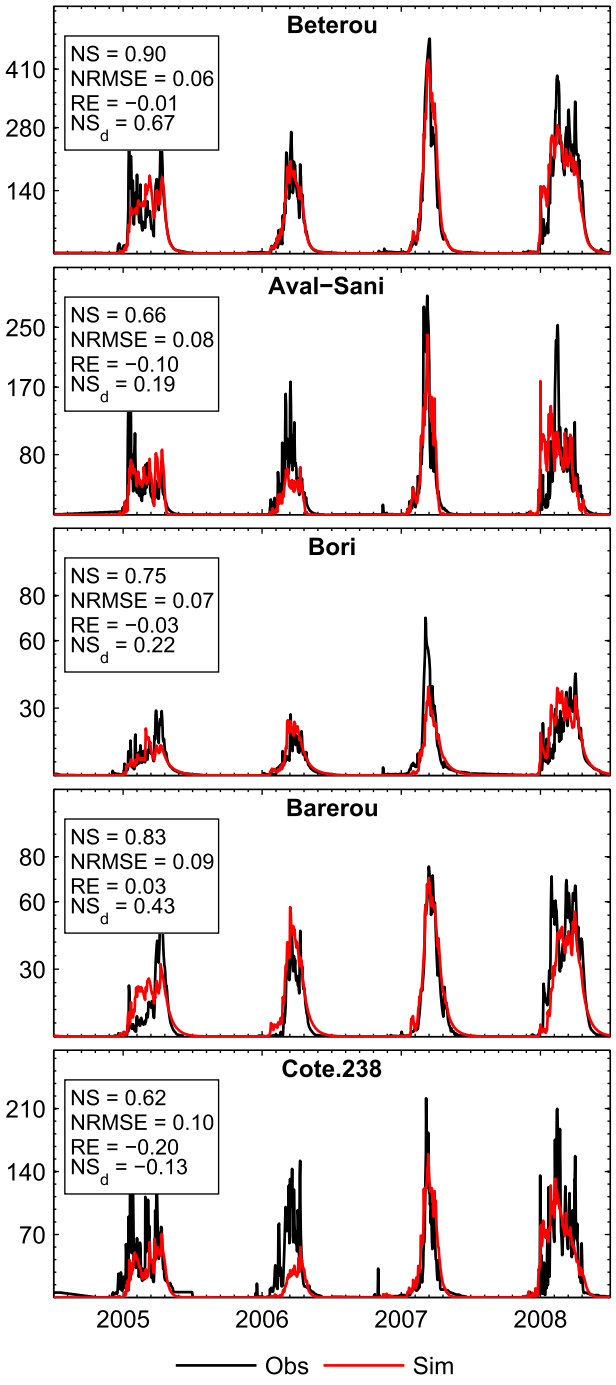

FIG. 8. As in Fig. 6, but for experiment 3 (i.e., calibration with observed streamflow data at five gauging stations individually).

The best overall results were obtained in experiment 3, for which basins were calibrated individually, and the incremental area of Beterou station was calibrated using optimal results for each upstream basin. This confirms the benefit of a spatially based calibration. Barerou station produced good simulated streamflow with NS = 0.83 and NS_d = 0.43 in experiment 3, in comparison to 0.77 and 0.21 in experiment 1 and 0.80 and 0.33 in experiment 2. Bori presented the best improvement from experiment 1 to experiment 3, with NS, RE, and NS_d values improving from 0.19, 41%, and −1.51 to 0.75, −3%, and 0.22. The worst results, which were obtained at Aval-Sani and Cote 238, can likely be explained by physical properties poorly represented by ECOCLIMAP in these areas. Even though a dense rain gauge network in the basin would reduce errors in the precipitation dataset, this forcing can also be a secondary explanation for errors in streamflow simulations. The evaluation of streamflow at four additional gauges (Tebou, Affon, Sarmanga, and Igbomakoro) reinforces the previous results that showed that the spatially distributed calibration performed in experiment 3 provided the best results. For example, NS, RE, and NS_d values at Affon evolved from 0.59, 024%, and 0.03 in experiment 2 to 0.66, −11%, and 0.20 in experiment 3. Figure 9 shows the results at four gauging stations used for the evaluation of experiment 3.

c. *Discussion of the parameterization*

As described in section 3a, the surface runoff τ_s time delay is a function of a surface runoff time delay factor T_r, defined by the Kirpich formula, and a spatially uniform surface runoff parameter r_d, which was parameterized. The base flow (τ_b) was also parameterized. Table 2 shows that approximately 30%–70% of the simulated base flow B is abstracted from the surface water budget and is diverted to deep water-table recharge. Overall, DWI values correspond to 6%–15% of rainfall P (see Table 3), which is slightly lower than but close to previous estimates of 10%–15%, as suggested by Séguis et al. (2011) on the basis of in situ measurements. A plausible explanation for the underestimated DWI/P ratios is that the contribution of R simulated by ISBA to the total river runoff is too high. As shown in Kamagaté et al. (2007) in a smaller catchment located in the northeastern Ouémé basin, most of the river discharge originates from the subsurface flow B'. According to those estimates, B' represents 68%–83% of the total river discharge; hence, the surface runoff only accounted for 17%–32% of the water volume flowing in the rivers. On the other hand, we found that R accounts for 47%–63% of river discharge.

A DWI of 41% of B (or f = 0.59), τ_b = 8 days , and p_r = 32 were obtained for experiment 1. The inclusion of four other stations in the optimization, as defined by experiment 2, had little impact on the parameters with respect to the values obtained in the first experiment: increases in both τ_b and p_r to 10.7 days and 39, respectively, and a reduction in f to 57% was obtained. As discussed above, these parameter sets can provide

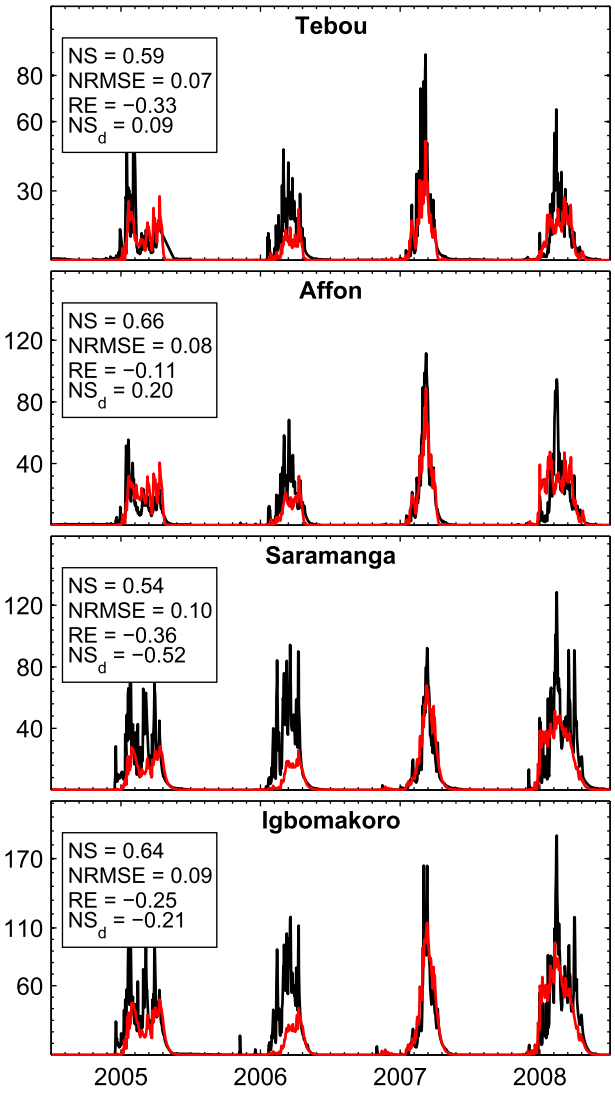

FIG. 9. As in Fig. 6, but for the four gauging stations used for the evaluation of experiment 3.

adequate simulated streamflow at Beterou, but other stations have lower statistical scores. Results obtained with experiment 3 suggest that the parameters are highly heterogeneous in space. Figure 10 shows the daily mean time series of streamflow from January to December for the 2005–08 period at the five stations used in the calibration procedure of experiment 3. Effects of parameter f are clearly seen at all of the stations, and the mean streamflow is reduced by a factor of approximately 2.5 at Beterou after the ARTS runs. The f values varied from 33% at Bori to 76% at Cote 238. The best improvements in terms of mean streamflow are observed at Beterou, Bori, and Barerou. This large difference is due to a higher loss of water toward the deep aquifer in the northeastern part of the basin. The analysis of observed

TABLE 3. Details on DWI estimates.

Station name	R (mm day^{-1})	B (mm day^{-1})	$1 - f$	DWI ratio (DWI/rainfall)
Beterou	0.16	0.68	0.41	0.09
Aval-Sani	0.16	0.70	0.3	0.07
Bori	0.16	0.67	0.67	0.15
Barerou	0.17	0.73	0.39	0.09
Cote 238	0.20	0.75	0.24	0.06

runoff ratios at Bori (Table 1) shows that, because of specific physical properties, the runoff capacity of this basin is lower than those observed at other locations. The relatively simplistic representation of these properties in both the ECOCLIMAP dataset and ISBA is likely responsible for the overestimation of the total runoff in this basin, and the low value of f acts as a correction factor.

The τ_b value varies from 1.9 days at Aval-Sani to 25.9 days at Bori. Barerou had a high τ_b value of 19.1 days while Beterou and Cote 238 had values similar to those obtained in experiments 1 and 2 (8.4 and 9.4 days, respectively). Because of the high baseflow rates, τ_b has a nonnegligible impact on the streamflow during the recession periods (period when rain ceases and streamflow drops and should be easily noticed at the end of rainy seasons). While $R + B$ from ISBA (i.e., without routing) drops to zero almost immediately when rain stops (see Fig. 10), water keeps flowing in the rivers for about 1 or 2 months, from October to December, depending on the basin. Simulations in experiment 3 could represent the recession periods at most stations, demonstrating the sensitivity of τ_b and how important it is to represent the baseflow water delay in a river routing modeling system. The exception is Aval-Sani, where an early drop of simulated streamflow is due to the low τ_b value obtained in experiment 3. This can be explained by a delayed total runoff peak simulated by ISBA at that station, forcing the optimization scheme to compensate it with a lower baseflow time delay.

5. Conclusions

The main objective of this paper is to assess the water budget as simulated by the current generation of land surface models (LSMs) over a basin with a monsoon climate. The current study focuses on the upper Ouémé River basin (Benin, West Africa) within the ALMIP-2 framework. In addition to evaluating the performance of LSMs, an attempt to identify key misrepresented processes is also performed. Groundwater dynamics and deep water-table recharge are examples of such processes and have been previously identified in the region

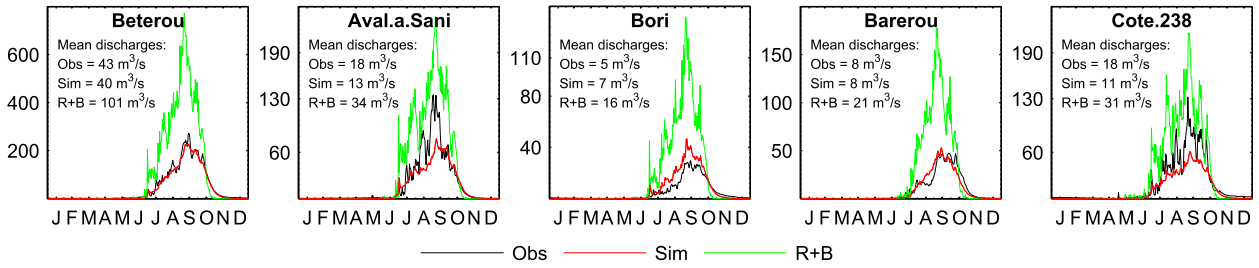

FIG. 10. Daily mean streamflow observations (Obs), ISBA-ARTS simulated streamflow (Sim) resulting from experiment 3 and ISBA total runoff ($R + B$) converted from mm day^{-1} to m^3 s^{-1} for comparison: (from left to right) Beterou, Aval-Sani, Bori, Barerou, and Cote 238.

(Kamagaté et al. 2007; Séguis et al. 2011). The water budget is simulated by the Interactions between Soil, Biosphere, and Atmosphere (ISBA) model (Noilhan and Mahfouf 1996) and surface runoff (R) and base flow (B) simulated by ISBA are used as forcing for the ALMIP-2 River Routing Scheme (ARTS), which has been specifically developed to generate streamflow in the study area. To evaluate the capability of ARTS to represent physical processes within the basin, three automatic calibration experiments were performed. The experiments were evaluated through the comparison of simulated discharges against observations at nine gauging stations within the basin. ARTS was developed with the main goal of routing R and B simulated by LSMs in offline mode at the mesoscale using a generic approach with a limited number of calibration parameters. The model combines a set of three reservoirs, representing baseflow water loss and the time delays for both R and B, with the Muskingum–Cunge method, representing the water transfer though the river network. Since the objective is to evaluate LSM water budgets at the mesoscale, ARTS only computes spatially distributed streamflow, which results in a relatively high computational efficiency. In this study, ARTS was run at the daily time step and 0.05° spatial resolution for the 2005–08 period. As mentioned before, ARTS is time efficient, and a single run in a standard computer takes only a few seconds. This is a great advantage while performing the automatic parameterization of numerous experiments. This study showed the utility of ARTS for computing streamflow from a single LSM, outlined an optimization strategy, and explored model sensitivity. The next phase of this work will be to use ARTS to study the water budget over this basin from an ensemble of ALMIP-2 LSMs.

To evaluate the parameterization based on the MOCOM-UA optimization algorithm, three experiments were performed, differing from each other according to the number of gauges used in the calibration procedures and the spatial distribution of parameters. Results demonstrate that the use of river routing schemes and observed streamflow is a straightforward way to evaluate the water budget provided by LSMs, and it also allows the identification of potentially misrepresented or missing processes at the river basin scale. The runoff simulated by ISBA overestimated observed streamflow in the entire basin (about 2.3 times at Beterou station). Plausible explanations for this overestimation are 1) the evidence of deep-water infiltration (DWI) as suggested by previous studies over West Africa and 2) the underestimation of simulated evapotranspiration owing to insufficient root depths. Another potential error source is the rainfall interpolation. However, owing to both the highly dense spatial distribution of the gauge network and the extensive evaluation of the rainfall product, potential errors are theorized to be too small to explain all of the runoff overestimation. As discussed above, most LSMs, including ISBA, do not represent deeper root zones, resulting in a lower evapotranspiration as a consequence of limited access to groundwater. A simple comparison against satellite-based products showed a slight underestimation of simulated ET, but it insufficient to explain such a difference between simulated and observed streamflow. More likely, as supported by observations in the study area, theses biases pointed to the necessity to consider DWI as an additional physical process in ISBA and other Earth system models.

In this study, we considered a robust solution based on an unconnected aquifer supplied by a fraction $1 - f$ of the base flow that leaves the system in the form of DWI, the remaining fraction f being transferred to the river along with the surface runoff. This scheme is consistent with field observations. Incidentally, this result shows that the simulated total runoff ($R + B$) often used in LSM modeling is not an appropriate approximation for river discharge in these tropical regions, as it is not consistent with the actual hydrological processes. The use of an offline scheme with an unconnected reservoir supplied by DWI was shown to significantly improve the simulations of streamflow at gauges within the basin. But

it is evident that this should be considered as a temporary solution until LSMs are improved to represent more detailed hydrological processes in the basin, notably more realistic groundwater representations. Indeed, the fact that trees ''seek out'' water at very deep depths to minimize stress during the dry season is perhaps a mechanism that is common to monsoon-dominated ecosystems and thus needs to be modeled if it is found in other such regions. This would imply a soil moisture memory that is potentially longer than what is currently represented in fully coupled global climate models, since most LSMs currently use soil depths in this region on the order of several meters at most (Boone et al. 2009b).

Future studies based on field measurements are recommended in order to better simulate the redistribution of base flow generated in land surface models. The deviation of a uniform and constant fraction of base flow out of the system is a very simplistic solution to represent such nonlinear processes. More complex solutions based on hydrogeological knowledge and considering spatial and temporal variability of parameter f should be used in future works. These solutions will potentially provide better streamflow estimates and, consequently, better overall simulations of the water budget.

Acknowledgments. A.C.V. Getirana was funded by EUMETSAT in the framework of the LSA SAF activities. This work is supported by the African Monsoon Multidisciplinary Analysis (AMMA) project. Based on a French initiative, AMMA was built by an international scientific group and has been funded by a large number of agencies in France, the United Kingdom, the United States, and Africa. The ALMIP-2 project is supported by AMMA, IRD (French overseas research institute), and INSU/CNRS (EC2CO/CYTRIX programme) French agencies. Observed data were obtained in the framework of the AMMA-CATCH Observatory (www.amma-catch.org) and with the contribution of the scientific and technical teams in Benin (IRD and Direction Générale de l'Eau, Cotonou). In particular, acknowledgements are due to Arnaud Zannou for providing streamflow data.

REFERENCES

Boone, A., J.-C. Calvet, and J. Noilhan, 1999: Inclusion of a third soil layer in a land-surface scheme using the force–restore method. *J. Appl. Meteor.,* **38,** 1611–1630, doi:10.1175/1520-0450(1999)038<1611:IOATSL>2.0.CO;2.

——, and Coauthors, 2004: The Rhône-Aggregation Land Surface Scheme Intercomparison project: An overview. *J. Climate,* **17,** 187–208, doi:10.1175/1520-0442(2004)017<0187:TRLSSI>2.0.CO;2.

——, and Coauthors, 2009a: AMMA Land Surface Model Intercomparison Project Phase 2 (ALMIP-2). *Gewex News,* Vol. 9, No. 4, International GEWEX Project Office, Silver Spring, MD, 9–10. [Available online at www.gewex.org/images/Nov2009.pdf.]

——, and Coauthors, 2009b: The AMMA Land Surface Model Intercomparison Project. *Bull. Amer. Meteor. Soc.,* **90,** 1865–1880, doi:10.1175/2009BAMS2786.1.

Boyle, D. P., H. V. Gupta, and S. Sorooshian, 2000: Toward improved calibration of hydrologic models: Combining the strengths of manual and automatic methods. *Water Resour. Res.,* **36,** 3663–3674, doi:10.1029/2000WR900207.

Canadell, J., R. B. Jackson, J. R. Ehleringer, H. A. Mooney, O. E. Sala, and E. D. Schulze, 1996: Maximum rooting depth of vegetation types at the global scale. *Oecologia,* **108,** 583–595, doi:10.1007/BF00329030.

Chow, V. T., 1988. *Applied Hydrology.* McGraw-Hill, 572 pp.

Coe, M. T., M. H. Costa, and E. A. Howard, 2008: Simulating the surface waters of the Amazon River basin: Impacts of new river geomorphic and flow parameterization. *Hydrol. Processes,* **22,** 2542–2553, doi:10.1002/hyp.6850.

Collischonn, W., D. Allasia, B. C. Silva, and C. E. M. Tucci, 2007: The MGB-IPH model for large-scale rainfall-runoff modelling. *Hydrol. Sci. J.,* **52,** 878–895, doi:10.1623/hysj.52.5.878.

Decharme, B., R. Alkama, F. Papa, S. Faroux, H. Douville, and C. Prigent, 2012: Global off-line evaluation of the ISBA-TRIP flood model. *Climate Dyn.,* **38,** 1389–1412, doi:10.1007/s00382-011-1054-9.

Depraetere, C., M. Gosset, S. Ploix, and H. Laurent, 2009: The organization and kinematics of tropical rainfall systems ground tracked at mesoscale with gages: First results from the campaigns 1999–2006 on the Upper Ouémé Valley (Benin). *J. Hydrol.,* **375,** 143–160, doi:10.1016/j.jhydrol.2009.01.011.

Descloitres, M., L. Séguis, A. Legchenko, M. Wubda, A. Guyot, and J.-M. Cohard, 2011: The contribution of MRS and resistivity methods to the interpretation of actual evapotranspiration measurements: A case study in metamorphic context in north Bénin. *Near Surf. Geophys.,* **9,** 187–200, doi:10.3997/1873-0604.2011003.

Desconnets, J. C., J. D. Taupin, T. Lebel, and C. Leduc, 1997: Hydrology of the HAPEX-Sahel Central Super-Site: Surface water drainage and aquifer recharge through the pool systems. *J. Hydrol.,* **188–189,** 155–178, doi:10.1016/S0022-1694(96)03158-7.

Farr, T. G., and Coauthors, 2007: The Shuttle Radar Topography Mission. *Rev. Geophys.,* **45,** RG2004, doi:10.1029/2005RG000183.

Gaiser, T., and Coauthors, 2008: Development of a regional model for integrated management of water resources at the basin scale. *Phys. Chem. Earth,* **33,** 175–182, doi:10.1016/j.pce.2007.04.018.

Geiger, B., C. Meurey, D. Lajas, L. Franchistéguy, D. Carrer, and J.-L. Roujean, 2008: Near real-time provision of downwelling shortwave radiation estimates derived from satellite observations. *Meteor. Appl.,* **15,** 411–420, doi:10.1002/met.84.

Getirana, A. C. V., M.-P. Bonnet, O. C. Rotunno Filho, W. J. Mansur, W. Collischonn, J.-L. Guyot, and F. Seyler, 2010: Hydrological modeling and water balance of the Negro River basin: Evaluation with observed data and spatial altimetry. *Hydrol. Processes,* **24,** 3219–3236, doi:10.1002/hyp.7747.

——, A. Boone, D. Yamazaki, B. Decharme, F. Papa, and N. Mognard, 2012: The Hydrological Modeling and Analysis Platform (HyMAP): Evaluation in the Amazon basin. *J. Hydrometeor.,* **13,** 1641–1665, doi:10.1175/JHM-D-12-021.1.

——, ——, ——, and N. Mognard, 2013: Automatic parameterization of a flow routing scheme driven by radar altimetry data: Evaluation in the Amazon basin. *Water Resour. Res.,* **49,** 614–629, doi:10.1002/wrcr.20077.

——, and Coauthors, 2014: Water balance in the Amazon basin from a land surface model ensemble. *J. Hydrometeor.,* doi:10.1175/JHM-D-14-0068.1, in press.

Giertz, S., B. Diekkrueger, and G. Steup, 2006: Physically-based modelling of hydrological processes in a tropical headwater catchment (West Africa)—Process representation and multi-criteria validation. *Hydrol. Earth Syst. Sci.,* **10,** 829–847, doi:10.5194/hess-10-829-2006.

Goldberg, D. E., 1989. *Genetic Algorithms in Search, Optimization, and Machine Learning*. Addison-Wesley-Longman, 412 pp.

Habets, F., R. Etchevers, C. Golaz, E. Leblois, E. Ledoux, E. Martin, J. Noilhan, and C. Ottle, 1999: Simulation of the water budget and the river flows of the Rhone basin. *J. Geophys. Res.,* **104,** 31 145–31 172, doi:10.1029/1999JD901008.

Kamagaté, B., L. Séguis, G. Favreau, J.-L. Seidel, M. Descloitres, and P. Affaton, 2007: Processus et bilan des flux hydriques d'un bassin versant de milieu tropical de socle au Benin (Donga, haut Ouémé). *C. R. Geosci.,* **339,** 418–429, doi:10.1016/j.crte.2007.04.003.

Kaptué Tchuenté, A. T., S. M. De Jong, J. L. Roujean, C. Favier, and C. Mering, 2011: Ecosystem mapping at the African continent scale using a hybrid clustering approach based on 1-km resolution multi-annual data from SPOT/VEGETATION. *Remote Sens. Environ.,* **115,** 452–464, doi:10.1016/j.rse.2010.09.015.

Kirpich, Z. P., 1940: Concentration time of small agricultural catchments. *Civ. Eng.,* **10,** 362.

Lebel, T., and Coauthors, 2009: AMMA-CATCH studies in the Sahelian region of West Africa: An overview. *J. Hydrol.,* **375,** 3–13, doi:10.1016/j.jhydrol.2009.03.020.

Leduc, C., J. Bromley, and P. Schroeter, 1997: Water table fluctuation and recharge in semi-arid climate: Some results of the HAPEX-Sahel hydrodynamic survey (Niger). *J. Hydrol.,* **188–189,** 123–138, doi:10.1016/S0022-1694(96)03156-3.

Le Lay, M., G.-M. Saulnier, S. Galle, L. Seguis, M. Metadier, and C. Peugeot, 2008: Model representation of the Sudanian hydrological processes: Application on the Donga catchment (Benin). *J. Hydrol.,* **363,** 32–41, doi:10.1016/j.jhydrol.2008.09.006.

Li, H., M. S. Wigmosta, H. Wu, M. Huang, Y. Ke, A. M. Coleman, and L. R. Leung, 2013: A physically based runoff routing model for land surface and earth system models. *J. Hydrometeor.,* **14,** 808–828, doi:10.1175/JHM-D-12-015.1.

Lohmann, D., and Coauthors, 1998: The Project for Intercomparison of Land-surface Parameterization Schemes (PILPS) phase 2(c) Red–Arkansas River basin experiment: 3. Spatial and temporal analysis of water fluxes. *Global Planet. Change,* **19,** 161–179, doi:10.1016/S0921-8181(98)00046-0.

Masson, V., and Coauthors, 2013: The SURFEXv7.2 externalized platform for the simulation of Earth surface variables and fluxes. *Geosci. Model Dev.,* **6,** 929–960, doi:10.5194/gmd-6-929-2013.

Miralles, D. G., T. R. H. Holmes, R. A. M. De Jeu, J. H. Gash, A. G. C. A. Meesters, and A. J. Dolman, 2011: Global land-surface evaporation estimated from satellite-based observations. *Hydrol. Earth Syst. Sci.,* **15,** 453–469, doi:10.5194/hess-15-453-2011.

Mu, Q., F. A. Heinsch, M. Zhao, and S. W. Running, 2007: Development of a global evapotranspiration algorithm based on MODIS and global meteorology data. *Remote Sens. Environ.,* **111,** 519–536, doi:10.1016/j.rse.2007.04.015.

——, M. Zhao, and S. W. Running, 2011: Improvements to a MODIS global terrestrial evapotranspiration algorithm. *Remote Sens. Environ.,* **115,** 1781–1800, doi:10.1016/j.rse.2011.02.019.

Noilhan, J., and J.-F. Mahfouf, 1996: The ISBA land surface parameterization scheme. *Global Planet. Change,* **13,** 145–159, doi:10.1016/0921-8181(95)00043-7.

Ponce, V. M., 1989: *Engineering Hydrology: Principles and Practices.* Prentice-Hall, 627 pp.

——, and V. Yevjevich, 1978: Muskingum–Cunge method with variable parameters. *J. Hydraul. Div.,* **104,** 1663–1667.

Redelsperger, J.-L., C. D. Thorncroft, A. Diedhiou, T. Lebel, D. J. Parker, and J. Polcher, 2006: African Monsoon Multidisciplinary Analysis: An international research project and field campaign. *Bull. Amer. Meteor. Soc.,* **87,** 1739–1746, doi:10.1175/BAMS-87-12-1739.

Richard, A., S. Galle, M. Descloitres, J.-M. Cohard, J.-P. Vandervaere, L. Séguis, and C. Peugeot, 2013: Interplay of riparian forest and groundwater in the hillslope hydrology of Sudanian West Africa (northern Benin). *Hydrol. Earth Syst. Sci.,* **17,** 5079–5096, doi:10.5194/hess-17-5079-2013.

Schaefli, B., and H. V. Gupta, 2007: Do Nash values have value? *Hydrol. Processes,* **21,** 2075–2080, doi:10.1002/hyp.6825.

Séguis, L., and Coauthors, 2011: Origins of streamflow in a crystalline basement catchment in a sub-humid Sudanian zone: The Donga basin (Benin, West Africa): Inter-annual variability of water budget. *J. Hydrol.,* **402,** 1–13, doi:10.1016/j.jhydrol.2011.01.054.

Trambauer, P., E. Dutra, S. Maskey, M. Werner, F. Pappenberger, L. P. H. van Beek, and S. Uhlenbrook, 2014: Comparison of different evaporation estimates over the African continent. *Hydrol. Earth Syst. Sci.,* **18,** 193–212, doi:10.5194/hess-18-193-2014.

Trigo, I. F., and Coauthors, 2011: The Satellite Application Facility on Land Surface Analysis. *Int. J. Remote Sens.,* **32,** 2725–2744, doi:10.1080/01431161003743199.

Tucci, C. E. M., 1998. *Modelos Hidrológicos.* ABRH-UFRGS, 669 pp.

Varado, N., I. Braud, S. Galle, M. Le Lay, L. Séguis, B. Kamagaté, and C. Depraetere, 2006: Multi-criteria assessment of the Representative Elementary Watershed approach on the Donga catchment (Benin) using a downward approach of model complexity. *Hydrol. Earth Syst. Sci.,* **10,** 427–442, doi:10.5194/hess-10-427-2006.

Vischel, T., T. Lebel, S. Massuel, and B. Cappelaere, 2009: Conditional simulation schemes of rain fields and their application to rainfall–runoff modeling studies in the Sahel. *J. Hydrol.,* **375,** 273–286, doi:10.1016/j.jhydrol.2009.02.028.

Yapo, P. O., H. V. Gupta, and S. Sorooshian, 1997: A multi-objective global optimization algorithm with application to calibration of hydrologic models. HWR Tech. Rep. 97-050, Dept. of Hydrology and Water Resources, University of Arizona, Tucson, AZ, 203 pp.

——, ——, and ——, 1998: Multi-objective global optimization for hydrologic models. *J. Hydrol.,* **204,** 83–97, doi:10.1016/S0022-1694(97)00107-8.